HENRY GRANJON PRIZE COMPETITION 2003
Co-Winner, Category B
"Materials behaviour and weldability"

MICROSTRUCTURE ASPECTS OF CREEP RESISTANT WELDED JOINTS

E. Letofsky
Graz University of Technology, (Austria)

ABSTRACT

A soft zone in the welded joint, negatively influencing the creep behaviour, was detected and localised in the intercritical zone of the heat affected zone (HAZ), limiting the long-time creep strength of welds. Energy-filtering transmission electron microscopy (EFTEM) has been used for imaging precipitates and grain boundary phases in the soft zone of the HAZ and in the weld deposit of advanced ferritic martensitic Cr steels. Due to different creep duration times at a temperature of 600°C, many different precipitates and grain boundary phases and a new type of Cr-V-Nb-N rich precipitation, the so-called modified Z phase emerge in the joint. The appearance of the Cr and V rich Z phase was followed by a decrease of the population of $M_{23}C_6$ and MX precipitates. According to these results a decrease of the creep strength in the soft zone of the HAZ beginning after about 10,000 h was found, which seems to be in connection with the observed microstructural changes. This effect must be taken into account in the design of welded components made from this type of materials. Basic investigations using mainly the Gleeble HAZ simulation technique corroborate a drop in the hardness (soft zone) and creep resistance that occurred in the inter critical zone of the HAZ, where the peak temperature reached a level of about 900-1,000°C (zone of α/γ–transformation). This and previous investigations have shown a drop in the creep resistance for the HAZ. Compared with the base material, reductions of the creep resistance in weld samples of about 20-25% have to be taken into account. At lower stress values, the fracture location shifts from the base material towards the softened intercritical zone of the HAZ (type IV cracking). The microstructure of the HAZ shows after stressed condition pores and micro-cracks in the softened intercritical zone (temperature between Ac_1 and Ac_3). A correlation between the creep resistance and the size distribution of particular particle populations could not be clearly proven. For the total evaluation of the microstructural development the reduction of the dislocation density and the recovery processes (formation and growth of subgrain boundaries) must be taken into account. The tests were made on cast G-X12 CrMoWVNbN 10.1.1 parent material and Cromocord 10M weld deposit

IIW-Thesaurus keywords: *Turbines; Castings; Creep resisting materials; High alloy steels; Parent material; Deposited metal; Heat affected zone; Microstructure; Stress rupture strength; Electron microscopes; Creep strength; Practical investigations; Reference lists.*

1 INTRODUCTION

In large castings for steam turbine components manufacturing, as well as in fabrication, welding is a standard procedure in the manufacturing process. The knowledge of the behaviour of welds during long-time service of the castings is of great importance. A soft zone in the welded joint, negatively influencing the creep behaviour, was detected and localised in the intercritical zone of the heat affected zone (HAZ), limiting the long-time creep strength of welds. Energy-filtering transmission electron microscopy (EFTEM) has been used for imaging precipitates and grain boundary phases in the soft zone of the HAZ and in the weld deposit of advanced ferritic martensitic Cr steels. Due to different creep duration times at a temperature of 600°C, many different precipitates and grain boundary phases such as chromium carbides ($M_{23}C_6$), vanadium nitrides, niobium carbonitrides (MX), Mo-W Laves phase and a new type of Cr-V-Nb-N rich precipitation, the so-called modified Z phase, emerge in the joint. The appearance of the Cr and V rich Z phase was followed by a decrease of the population of $M_{23}C_6$ and MX precipitates. According to these results a decrease of the creep strength in the soft zone of the HAZ beginning after about 10,000 h was found, which seems to be in connection with the observed microstructural changes. This effect must be taken into account in the design of welded components made from this type of materials [1-4].

Doc. IIW-1612-03 (ex-doc. IX-2055-03) recommended for publication by Commission IX "Behaviour of metals subjected to welding"

2 MATERIALS INVESTIGATED AND EXPERIMENTAL PROCEDURE

Table 1 shows the chemical composition in weight-% of the materials investigated [(BM): base material; G-X12 CrMoWVNbN 10.1.1 (G-X12), (WM): weld deposit; Cromocord 10M].

For a successful service application and acceptance in practice, the weldability and the long-time behaviour of the newly developed materials is one of the most important aspects. In Fig. 1 the creep rupture strength values of the G-X12 CrMoWVNbN 10.1.1 cast parent material at 600°C are compared with the creep rupture strength values of weld specimens. It can be observed that at higher temperatures the creep rupture strength of the weld samples is significantly lower than that of the base material.

Investigations are concentrated on metallographic investigations, hardness tests, and creep rupture tests of long-term stressed welded joints.

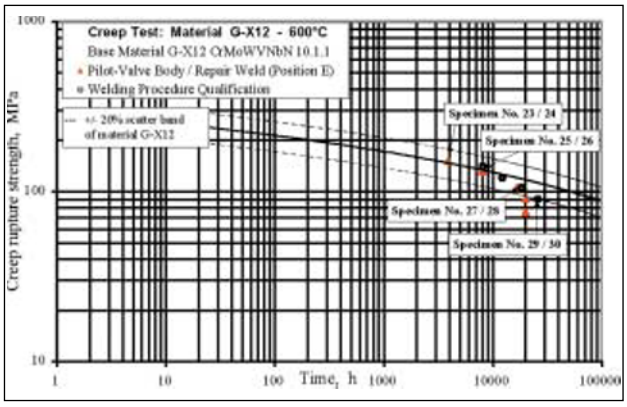

Fig. 1. Results of the creep tests on G-X12 cast parent material and welded joints at 600°C (the Nos. indicate the respective microstructures).

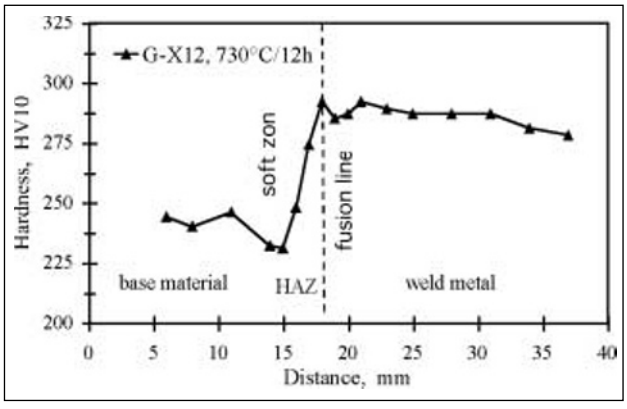

Fig. 2. Hardness of weld after post weld heat treatment of G-X12.

The hardness profile across G-X12 welds shows that this type of steel forms a soft zone in the HAZ after post-weld heat treatment (PWHT) (Fig. 2). The hardness in the zones was found to be ≈20 HV10 lower than that of the unaffected base material. Investigations on tempered simulated weld specimens show that the hardness is not influenced by thermal cycles with peak temperatures up to about 850°C. In the range of peak temperatures between 900 and 1,000°C in the materials, the zone of α/γ-transformation, a minimum hardness can be observed (soft zone). At higher peak temperatures this effect seems to be overcome [5, 6]. Constant strain rate tests applied on simulated HAZ materials at 600°C (after Steen) show, for different peak temperatures in the range of α/γ-transformation, a minimum of stress σ^* (Fig. 3).

3 RESULTS AND DISCUSSION

3.1 Microstructural investigation on creep rupture tested cruciform weld samples

Figure 1 shows the current status of creep tests performed on welded joints produced by shielded metal arc welding (SMAW). These results are compared with the creep rupture strength values of the parent material G-X12. It can be observed that, as time increases, the creep rupture strength of crossweld samples becomes significantly lower than that of the base material. The hardness profiles for the samples investigated are shown in Fig. 4.

Fig. 5 shows microstructural investigations related to the soft zone behaviour on creep tested crossweld samples. At high stress levels the fracture is located in the base material (Fig. 5). As the applied stress decreases and rupture time increases, the fracture location shifts from the base material (Fig. 4a) into the intercritical zone

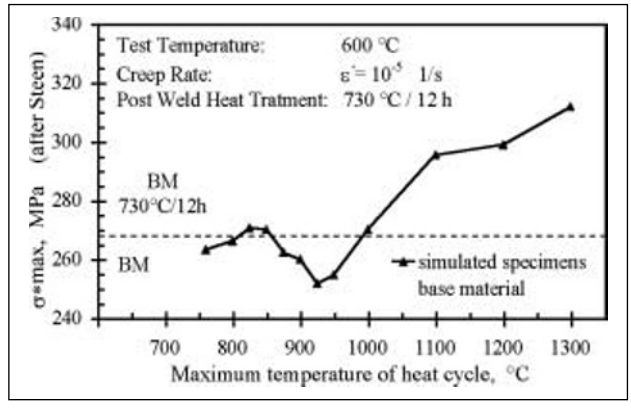

Fig. 3. Results of constant strain rate tests on specimens of G-X12 subjected to welding thermal cycle simulation treatment followed by tempering.

Table 1. Chemical composition of materials investigated.

	C	Cr	Ni	Mo	W	V	Nb	N
BM	0.12	10.5	0.90	0.99	0.99	0.22	0.08	0.05
WM	0.12	10.0	0.95	1.06	0.95	0.22	0.09	0.04

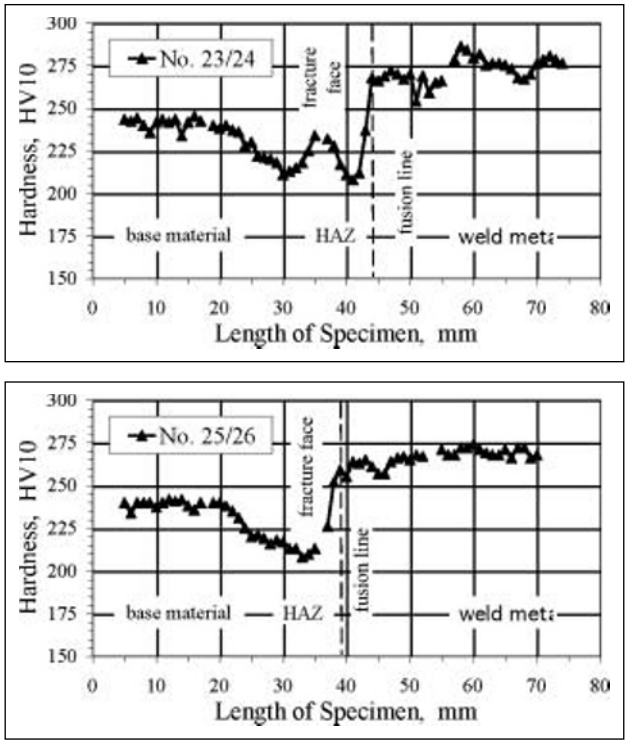

Fig. 4. Hardness profile of creep samples (G-X12 welded joint [SMAW]).

(peak temperature between A_C1 and A_C3) in the HAZ (Fig. 4b). The microstructure of the HAZ shows cavities and micro-cracks.

3.2 Energy-filtering transmission electron microscopy (EFTEM)

The exact knowledge of the microstructure is essential for investigating the microstructural evolution at long-term service and their resulting change in properties.

It is not possible to distinguish the different precipitates purely by their shape and appearance in the TEM bright-field image. A reliable sectioning of the general distribution shown in individual distributions is therefore hardly possible with justifiable expenditure. The EFTEM method [9] allows visualising the distribution of the different precipitates in the HAZ and the weld deposit. If the precipitate types differ clearly in their chemical composition, as in the concrete case of the Cr-content of the $M_{23}C_6$-carbides, the Mo-content and the W-content of the Laves phase and the V-content of the VN, they can be visualized by the EFTEM method [10] and subsequently evaluated by image analysis. This procedure also gives information on the size distribution of the particular particle populations.

For this investigations creep samples made of a production weld from a G-X12 casting were used. TEM bright-field images (Fig. 6) and images processed by superimposing the energy-filtering TEM elemental distribution images of elements Fe, Cr, Mo, W, V, Nb, C, N (Fig. 7) were investigated for the HAZ (soft zone) of the cast material G-X12 CrMoWVNbN 10-1-1 and the weld deposit (Cromocord 10M). Figs. 6 and 7 show the as-received condition and the long-term stressed condition at 600°C. For investigations of the soft zone area a target preparation was necessary (see Fig. 5).

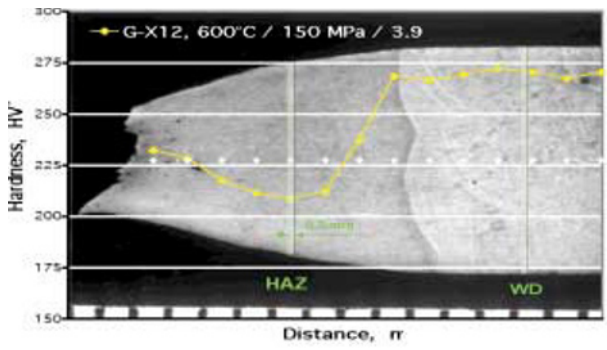

Fig. 5. Fracture location and hardness profile of weld sample: specimen no. 23/24 (from Fig. 1).

3.3 Data evaluation

Figures 8 and 9 show the quantitative distribution of precipitations in the as-received condition and the specimen stressed for 26,000 h at 600°C. A log-normal distribution was adapted to the histogram resulting from the classification [2, 4]. This procedure was carried out for the Cr-rich $M_{23}C_6$ carbides (Cr-element distribution images), V-rich VN precipitates (V-element distribution images), Mo- and W-rich Laves phase (Mo-element distribution images) and the Cr-V-N-Nb rich Z phase (combination between the Cr-, V- and N-element distribution images). A reliable determination of the distribution of the

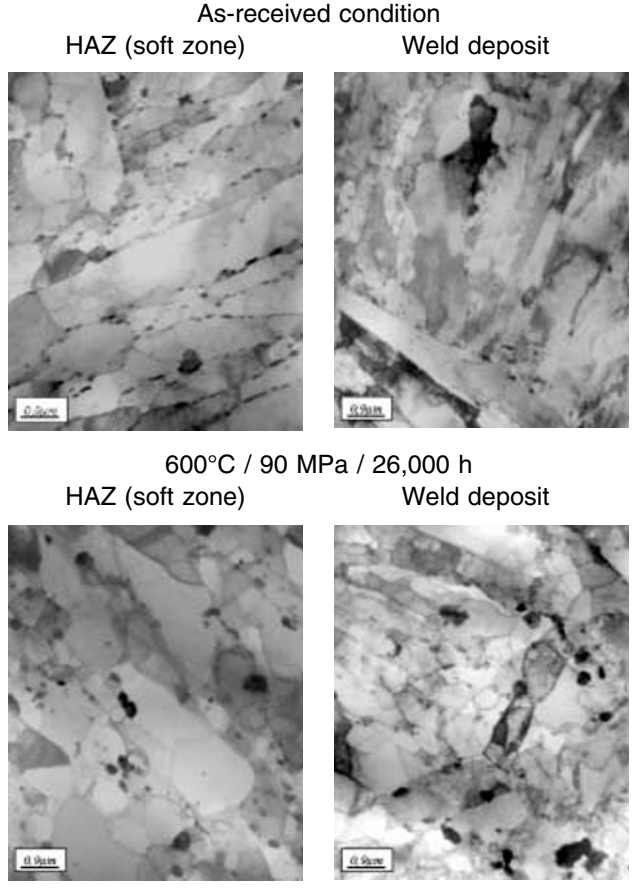

Fig. 6. G-X12 TEM – bright-field images; [9, 12].

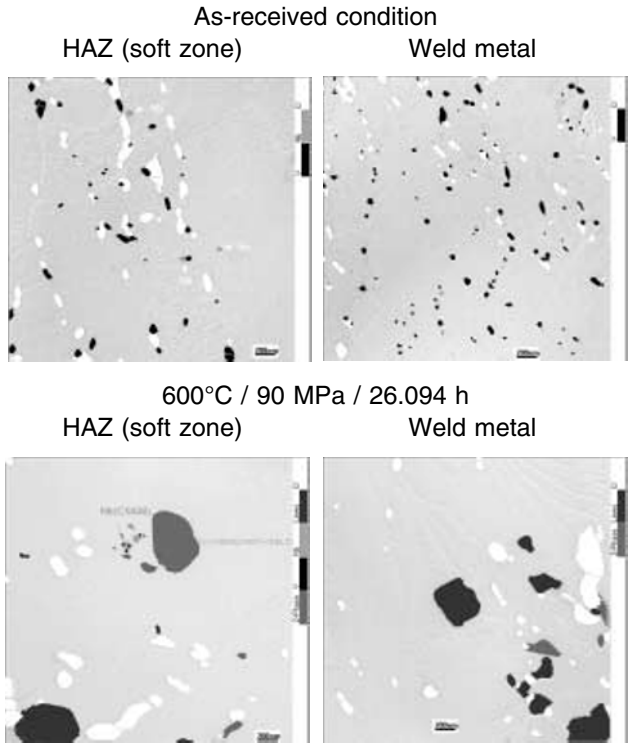

Fig. 7. Images processed by superimposing the energy-filtering TEM elemental distribution images (Fe, Cr, Mo, W, V, Nb, C, N) for G-X12 HAZ (soft zone) and Cromocord 10M weld deposit [9, 12].

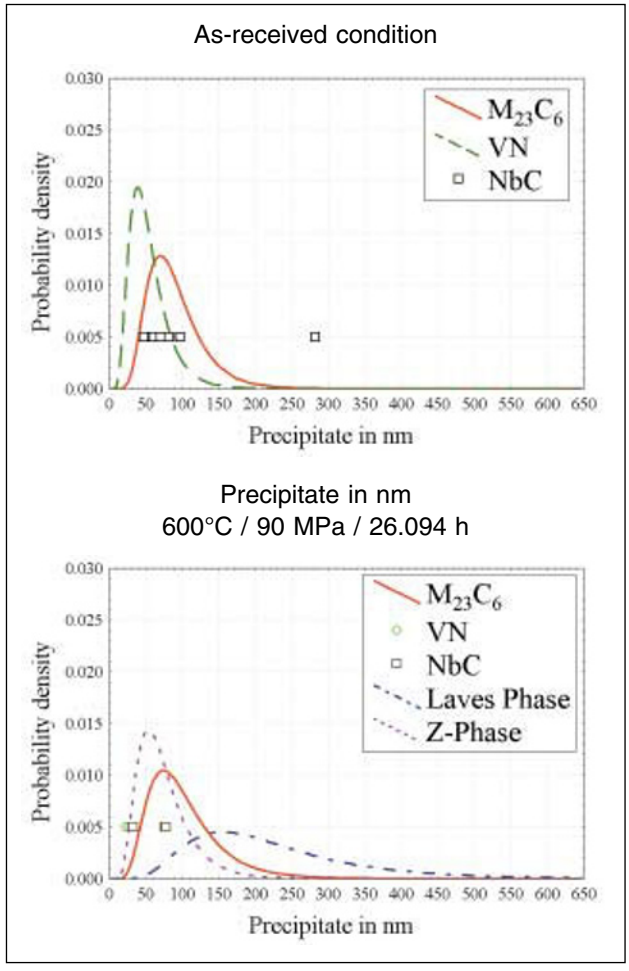

Fig. 8. Comparison of the distribution of the different particles analysed by EFTEM (G-X12, HAZ (soft zone)).

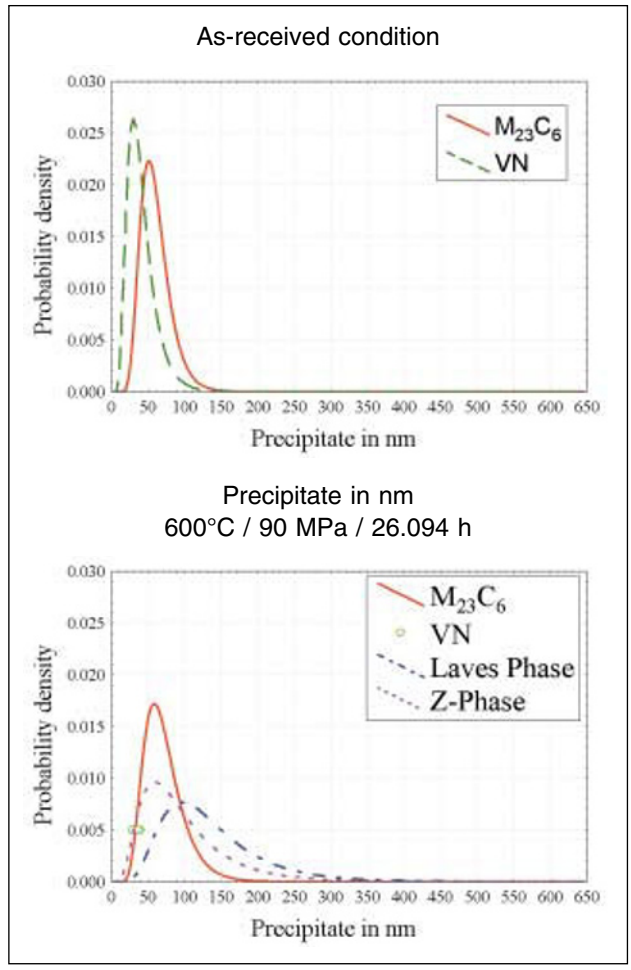

Fig. 9. Comparison of the distribution of the different particles analysed by EFTEM (Cromocord 10M, weld deposit).

Laves phase was however not possible with long-term run specimens because of the lack of sufficient numbers of the highly coarsened Laves phase in the volume investigated. To get nevertheless a notion of the distribution of the Laves phase and to limit the research expenditures, the results of the EFTEM investigation with long-term run specimens were combined with those of the TEM investigation. The measured distribution contains especially $M_{23}C_6$ carbides and Laves phase. The V-enriched MX particles are barely detectable in the bright-field image. Therefore, when using conventional evaluation of TEM bright-field images, these particles are not considered.

The results of the individual measurements are however reported in the distribution graphs (see Fig. 8). The distribution in the weld deposit is narrower as compared with that in the soft zone of the HAZ. With longer duration times a coarsening and coagulation of the Laves and Z phases could be observed. The Cr-rich $M_{23}C_6$ and V-rich MX precipitates do not coarsen. The appearance of the Cr- and V-rich Z phase was followed by a decrease of the population of $M_{23}C_6$ and MX precipitates.

Fig. 10 shows a quantitative analysis of the number of particles per unit volume $N_V = N_A / (t + d)$ [13], where N_A is the number of particles per unit area, t is the thick-

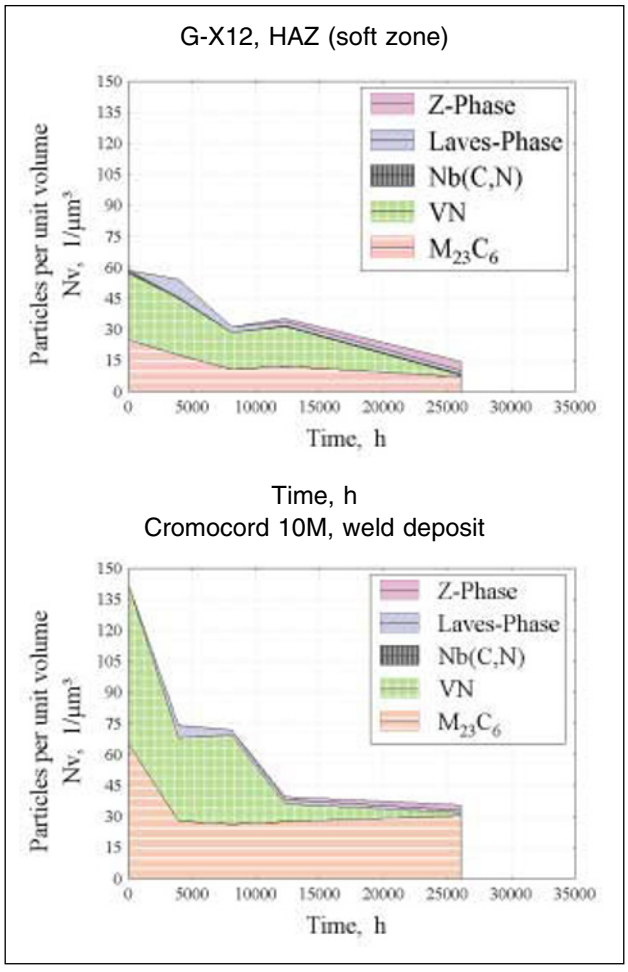

Fig. 10. Particles per unit volume of $M_{23}C_6$, MX, Laves and Z phases.

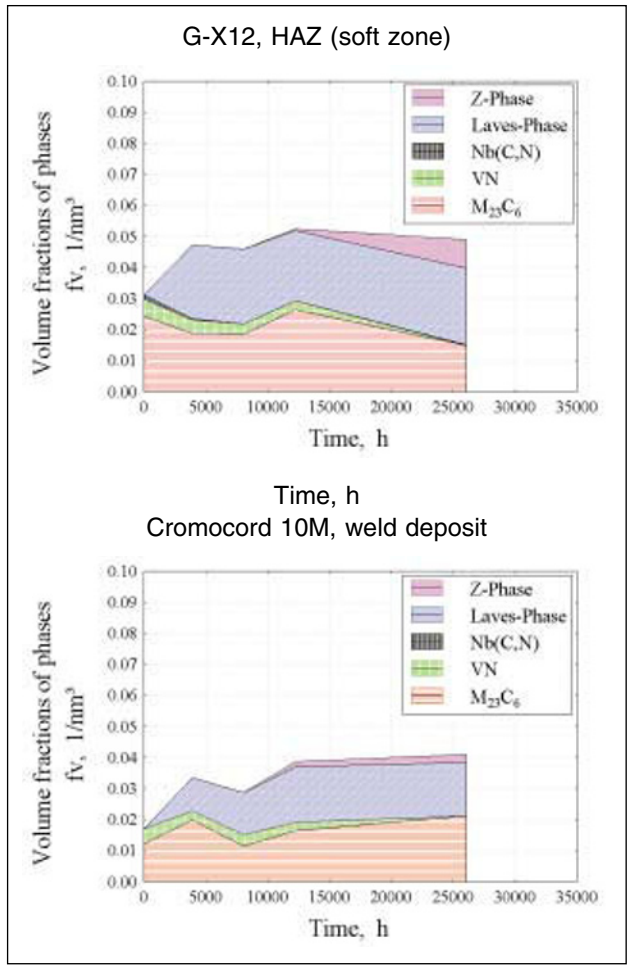

Fig. 11. Volume fractions of $M_{23}C_6$, MX, Laves and Z phases.

ness of the foil and *d* is the average equivalent diameter. The average foil thickness *t* for each material condition was derived from thickness maps produced from an unfiltered image and a zero-loss image.

The number of all detected particles is higher in the weld deposit than in the HAZ (soft zone). In the weld deposit the number of $M_{23}C_6$ and MX particles are dropping in the early period. For longer periods only the number of detected MX particles decreases. The Z phase particles number increases after about 10,000 hours.

Using EFTEM, the volume fractions of $M_{23}C_6$, MX, Laves and Z- phases were derived from the measured diameters using the following equation [14]

$$f_V = K\, V_P\, N_V$$

where *K* is a truncation correction factor assuming spherical particles of uniform size, V_P is the average volume of the measured particles and N_V is the number of particles per unit volume. The correction factor *K* was calculated by Lundin *et al.* [14]. For the MX precipitates $K = 1.1$ and for the $M_{23}C_6$ precipitates $K = 1.2$. For the Laves and Z phase the factor *K* was adopted with $K = 1.2$.

The results are given in Fig. 11. For the HAZ (soft zone) a higher amount of f_V was calculated as compared with the weld deposit. The volume fractions of MX particles decreases with time. The volume fraction of $M_{23}C_6$ particles decreases in the HAZ (soft zone) but not in the weld deposit. The Laves phase volume fraction increases on shorter duration times and becomes stable during longer exposure periods. The volume fraction of the Z phase increases with time.

According to these results the beginning of the decrease of the creep strength around 10,000 h can be seen in connection with these observed microstructural changes. For long-term creep tested specimens, a similar trend of the microstructural evolution in the newly developed tungsten-containing materials can also be expected. Appropriate investigations are in progress.

4 SUMMARY AND OUTLOOK

Basic investigations using mainly the Gleeble HAZ simulation technique corroborate a drop in the hardness (soft zone) and creep resistance that occurred in the inter critical zone of the HAZ, where the peak temperature reached a level of about 900-1,000°C (zone of α/γ-transformation). This and previous investigations [5-8] have shown a drop in the creep resistance for the HAZ. Compared with the base material, reductions of the creep resistance in weld samples of about 20-25% have to be taken into account. At lower stress values, the fracture location shifts from the base material towards

the softened intercritical zone of the HAZ (type IV cracking). The microstructure of the HAZ shows after stressed condition pores and micro-cracks in the softened intercritical zone (temperature between Ac_1 and Ac_3).

A correlation between the creep resistance and the size distribution of particular particle populations could not be clearly proven. For the total evaluation of the microstructural development the reduction of the dislocation density and the recovery processes (formation and growth of subgrain boundaries) must be taken into account.

ACKNOWLEDGEMENT

This work was a part of the European Action COST501, Round III and COST522, and was supported by the Austrian Research Fund (FFF) which is gratefully acknowledged.

REFERENCES

1. H. Cerjak, P. Hofer, P. Warbichler, Microstructural evaluation of aged 9-12% Cr Steels containing W, Proc. Materials Ageing and Component Life Extension, Conf. Milano 10-12 October (1995).

2. P. Hofer, Mikrostrukturelle Analyse als Basis für die Entwicklung neuer Kraftwerkswerkstoffe am Beispiel von G-X12 CrMoWVNbN 10-1-1, Doctoral Thesis, TU-Graz (1999).

3. H. Cerjak, V. Foldyna, P. Hofer, B. Schaffernak, Microstructure of Advanced High Chromium Boiler Tube Steels, in: Microstructural development and stability in high chromium ferritic power plant steels, eds.: Strang A., Gooch D.J.: The Institute of Materials (1997), pp. 145-158.

4. P. Hofer, H. Cerjak, P. Warbichler, Beitrag zur Quantifizierung der Entwicklung betriebsbedingter Ausscheidungen in neuen 9 bis 12% Cr-Stählen am Beispiel G-X12CrMoWVNbN-10-1-1, Prakt. Met. Sonderband 30 (1999), pp. 165-172.

5. H. Cerjak, E. Letofsky, Microstructural Aspects of the Weldability of Advanced 9-12% Cr-Steels, 5th Inter. Conf. on Tends in Welding Research, 1-5 June 1998, Pine Mountain, GA, USA.

6. H. Cerjak, E. Letofsky, G. Feigl, P. Pichler, Characterisation of the Weldability and Behaviour of the Heat Affected Zone for Steel E911, in Materials for Advanced Power Engineering 1998, eds.: J. Lecomte-Beckers, F. Schubert, P.J. Ennis: Forschungszentrum Jülich, Energietechnik, pp. 401-410.

7. W. Bendick, K. Haarmann, G. Wellnitz, M. Zschau, Eigenschaften der 9- bis 12-%-Chromstähle und ihr Verhalten unter Zeitstandbeanspruchung, VGB Kraftwerkstechnik 73, Heft 1 (1993).

8. F. Brühl, Verhalten des 9%-Chromstahles X10CrMoVNb9-1 und seiner Schweißverbindungen im Kurz- und Langzeitversuch, Doctoral Thesis, TU-Graz (1989).

9. P. Warbichler, F. Hofer, P. Hofer, E. Letofsky, On the application of energy-filtering TEM in materials science: III. Precipitates in steel, Micron Vol. 29, No. 1 (1998), pp. 63-72.

10. F. Hofer, P. Warbichler, W. Grogger, Ultramicroscopy 59 (1995), pp. 15-31.

11. A. Strang, V. Vodarek, Z phase formation in martensitic 12CrMoVNb steel, Materials Science and Technology, Vol.12 (1996), pp. 552-556.

12. H. Cerjak, P. Hofer, B. Schaffernak, Beitrag zur Quantifizierung der Entwicklung betriebsbedingter Ausscheidungen in neuen 9 bis 12% Cr-Stählen, 20. Vortragsveranstaltung “Langzeitverhalten warmfester Stähle und Hochtemperaturwerkstoffe”, VDEh Düsseldorf, 28.11.1997, pp. 56-63.

13. E.E. Underwood: Quantitative stereology, Aaddison-Wesley, Massachusetts, 1970.

14. L.M. Lundin, M. Hättestrand, H.O. Andrén, Redistribution of elements during ageing and creep testing of 9-12% chromium steels, in PARSONS 2000 Advanced Materials for 21st Century Turbines and Power Plant, eds.: A. Strang *et al.*, IOM Communication (2000), pp. 601-617.